Cooperative Regulation of Imbalances in Three-Phase Four-Wire Microgrids Using Single-Phase Droop Control and Secondary Control Algorithms

Enrique Espina, *Student Member, IEEE*, Roberto Cárdenas-Dobson, *Senior Member, IEEE*, Mauricio Espinoza-B., *Student Member, IEEE*, Claudio Burgos-Mellado, *Student Member, IEEE*, and Doris Sáez, *Senior Member, IEEE*

***Abstract*—Collaborative control of power converters operating in microgrids with unbalanced single-phase loads is difficult to achieve, considering that the voltages and currents have positive-, negative-, and zero-sequence components. In this paper, a new control scheme for collaborative control of four-leg microgrids is proposed. The main advantage of the proposed methodology is simplicity, because the sharing of the powers produced by the positive-, negative-, and zero-sequence voltage and currents is simple to achieve using the easy to implement and well-known droop control algorithms, i.e., as those based on P–ω and Q–v droop control. The proposed droop algorithms do not require high bandwidth communication channels and the application of virtual impedances, whose design usually demands extensive simulation work, is not required. Three secondary control systems are also analyzed, discussed, and implemented in this paper to regulate the frequency, voltage, and phase at the point of common coupling (PCC), to achieve a balanced 50-Hz three-phase voltage supply in the PCC during steady-state operation. For these secondary control systems, single-phase phase-locked loop based on quadrature signal generators are implemented. Small signal modeling and design are discussed in this paper. A microgrid prototype of ≈5 kW, implemented using two power converters of 3 kW (each), is used to experimentally validate the proposed algorithms.**

***Index Terms*—Droop control, four-leg converters, unbalanced microgrids (MGs), secondary control.**

I. Introduction

MICROGRIDS (MGs) are an attractive solution for electrification in rural areas, industrial parks, commercial, and institutional campuses, among other places [1]–[4]. An MG could be composed of a cluster of loads, distributed generators (DGs), and energy storage systems (ESSs), connected to the main ac power system at the distribution level at the point of common coupling (PCC) [4]. These components may be single- or three-phase devices and usually, for low-voltage distribution systems, a four-wire microgrid is required to provide a neutral point [5]. When this interface is a four-leg topology, the neutral connection is provided by a dedicated power converter leg. This approach is usually preferred for creating the neutral point of connection since it does not require either a bulky transformer or large dc link capacitors. Moreover, the control flexibility achieved with a four-leg converter, where each phase can be independently controlled, is much higher [6], [7].

Cooperative sharing of active (P) and reactive (Q) power has been widely studied and it can be achieved using droop control [3]. However, there is no straightforward solution to collaborative sharing in microgrids with strong imbalances and zero-sequence components. In unbalanced microgrids, overloading of a phase could reduce the power capability of the whole distributed generating unit, (e.g., by reaching the thermal limit in a single phase) unless the imbalance is either eliminated or shared with the other generating units [8]–[10]. Moreover, very few papers discuss collaborative control systems for four-wire microgrids, where the imbalances are produced not only by the presence of negative sequence components but also by the zero-sequence voltages and currents produced by single-phase loads [8], [11]. To achieve collaborative control, at least two approaches can be utilized. First is to eliminate the imbalances using active power filters and then droop control is applied to the already balanced system [9], [12]–[14]. However, active power filters constitute additional hardware and higher costs. The second and more cost-effective approach is to use the residual capacity of the existing power converters to implement collaborative power-sharing control strategies that can be applied to microgrids with imbalances in voltages and currents, thus maximizing the hardware utilization [15]–[19].

In [15], the unbalanced output voltage of the inverters is compensated by adding a negative sequence voltage component to the control loop references. However, these compensating signals depend on the load characteristics and it is difficult to calculate them in MGs with a high number of converters and with variable loads. In [17], a method for compensating harmonics and imbalances in an MG is proposed, which modifies both a

Manuscript received November 5, 2018; revised January 13, 2019 and March 31, 2019; accepted May 3, 2019. Date of publication May 19, 2019; date of current version November 12, 2019. This work was supported in part by FONDECYT 1170683, in part by CONICYT-PIA-FB0816, and in part by the Basal Project FB0008. The work of E. Espina was supported by CONICYT-PCHA/Doctorado Nacional/2017-21171858. Recommended for publication by Associate Editor M. Molinas. *(Corresponding author: Roberto Cardenas-Dobson.)*

E. Espina, R. Cárdenas-Dobson, C. Burgos-Mellado, and D. Sáez are with the Department of Electrical Engineering, University of Chile, Santiago 2007, Chile (e-mail: eespina@uchile.cl; claudioburgos87@gmail.com; rcardenas@ing.uchile.cl; dsaez@ing.uchile.cl).

M. Espinoza-B. is with the Faculty of Engineering, University of Costa Rica, San Pedro 11501–2060, Costa Rica (e-mail: maeb@ieee.org).

Color versions of one or more of the figures in this paper are available online at http://ieeexplore.ieee.org.

Digital Object Identifier 10.1109/TPEL.2019.2917653

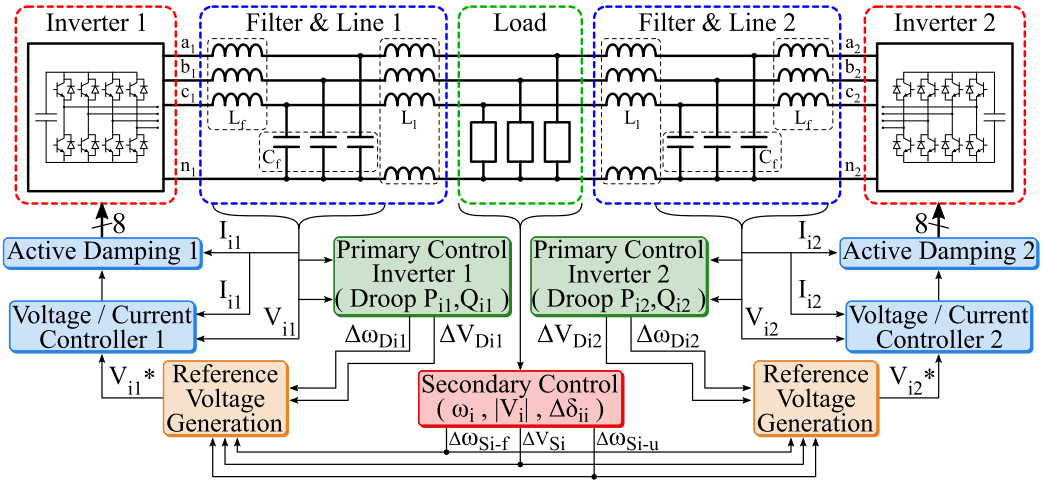

Fig. 1. Proposed three-phase four-wire microgrid control system.

virtual impedance loop and the inner voltage control loop. The method is effective; however, it is more suitable for a single DG operation. In [18], a cooperative method for compensating unbalanced voltages at the inverters outputs is proposed. The goal is to use the remaining VA capability of the converters as part of a negative sequence droop control scheme. However, the cooperative performance is strongly affected by the line impedances. In [19], a control method for reducing the voltage imbalances at the outputs of the inverters is proposed. The voltage compensation introduces negative sequence currents through the current-controlled converters. However, this method is hardly suitable for voltage-controlled converters. Notice that in [15]–[19], the zero-sequence components are not considered. The imbalance is represented by the negative sequence voltages and currents only.

In this paper, the application of frequency and voltage droop control systems, per phase, on a microgrid based on four-leg power converters is proposed. The control is based on the layers-based control structure proposed for microgrids (see [20]). The droop schemes are augmented by three secondary control systems designed to achieve 50-Hz operation and balanced voltages (at the PCC) in steady-state conditions. Tertiary control systems are not considered in this paper. The proposed methodology is proposed for three-phase four-wire microgrids where small transient variations in the voltages and frequencies of each phase can be tolerated by the four-wire three-phase unbalanced load connected to the PCC. For instance, in small rural villages located at the south of Chile (see [21]), which are usually isolated from the main grid, with the energy consumption being based on single-phase loads (typically used in households), e.g., lighting systems, electric heating, etc. These loads can tolerate relatively long transient variations in the frequency, phase, and magnitude of the voltages. Moreover, as discussed in Section III, there are some typical equipment that can operate with short transients of variable frequencies in the phase-to-neutral voltages, e.g., converter-fed drives and step-up/step-down transformers.

The contributions of this paper can be summarized as follows.

1) The main advantage of the proposed control system is simplicity. The control algorithms previously discussed in the literature for power sharing in four-leg unbalanced microgrids are typically based on separating the positive, negative, and zero-sequence components of the voltages and currents (which is not simple to achieve in the presence of noise and harmonic distortion), for instance, for the utilization of separate droop control algorithms to share the power in each sequence [15]. The utilization of virtual impedances for each sequence has also been reported [8]. However, the problem of this methodology is that the virtual impedances required are dependent on the operating point of the four-leg microgrid. Typically to tune the virtual impedances, extensive and time-consuming simulation work is required (see [8], [10], and [15]) or the application of genetic algorithms (see [16]) to optimally distribute the collaborative compensation efforts.
   In this paper, it is demonstrated that power sharing could be easily achieved using droop control applied to each phase. Droop control is a well-known methodology, simple to design and implement [20].
2) In this paper, new secondary control systems, designed to supply the load with balanced voltages, are proposed and extensively discussed. Using this control methodology, in steady-state operation, the voltages at the PCC do not have negative- and zero-sequence components. On the other hand, the control methods based on virtual impedances (see [9], [12]–[14], and [22]) are not designed to eliminate completely the voltage imbalances at the PCC. This is further corroborated by the simulation results presented in Section V-A of this paper.
3) Using the proposed droop per phase control system, the load connected in each phase of the PCC is shared between the converters as a function of their nominal power. This is complex to achieve by the control methods based on virtual impedances that are proposed in the literature [9], [12].
4) Small signal models and the design of the control systems are extensively discussed in this paper.

The control systems proposed in this paper are shown in Fig. 1. The microgrid is composed of four-leg power converters, each

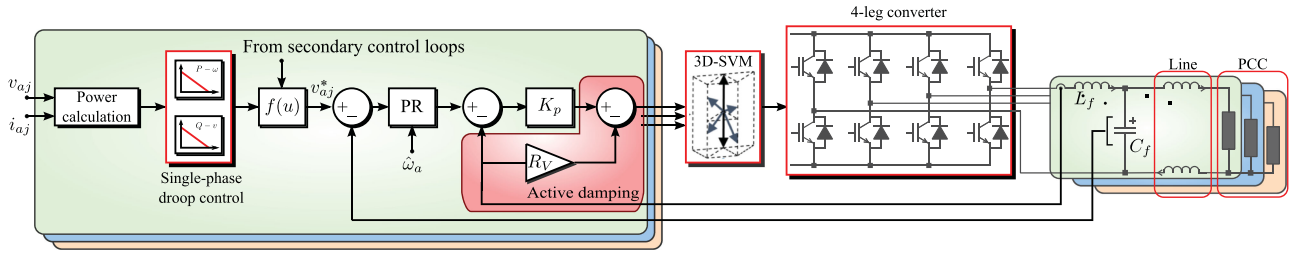

Fig. 2. Primary and inner control system of each four-leg converter.

one cascaded with an *LC* filter (L_f and C_f), and connected through an inductive line (L_l) to the PCC with a central load. An inductance is required in the neutral wire to reduce the effects of any zero-sequence voltage difference between neutral points of different power converters. Both inverters are controlled using three-dimensional (3-D) space vector modulation [6] and resonant controllers (RCs) with an active damping strategy [23] to provide extra damping to the *LCL* plant. Because droop control is applied per phase, there are short transient-variations on the single phase operating frequency and voltage amplitude around the nominal value. Therefore, droop control per phase has to be augmented with three secondary control systems designed to maintain the PCC voltages operating at the nominal frequency with equal-amplitude voltages and with a phase shift of $2\pi/3$ between them. In this paper, the secondary control systems are denominated, frequency secondary control system, angle secondary control system, and voltage amplitude secondary control system.

The remainder of this paper is organized as follows. The primary and inner control strategies are discussed in Section II. The effects of operating the microgrid with slightly different frequencies in each phase are analyzed in Section III, considering a vector approach. The three secondary control strategies proposed in this paper are presented and analyzed in Section IV. Additionally, small signal models of the quadrature signal generators (QSGs) and phase-locked loop (PLL), required for the design and implementation of the secondary control systems, are also introduced in Section IV. Simulation results are presented in Section V. Experimental results obtained from a 6-kW four-wire experimental prototype are presented and extensively analyzed in Section VI. Finally, in Section VII, an appraisal of the proposed methodologies is presented at the conclusions.

II. Primary Control Systems

As mentioned in Section I, the control algorithms used in microgrid systems are typically implemented using a hierarchical approach, where several control layers are implemented (see [20]). Namely, primary control systems, secondary control systems, etc. In this section, the primary controllers are discussed, whereas the proposed secondary control systems are discussed in Section III.

The primary control system is designed for independent regulation of voltages and frequencies in each of the four-leg converter phases, as depicted in Fig. 2. In the proposed methodology, each phase considers droop control (both P–ω and Q–V), nested voltage/current control loops, and a virtual resistance R_v to provide active damping at the converter output (see [24]). To tune R_v, it is assumed that the impedance of the load is relatively large when compared with the other impedances represented by L_f and C_f (i.e., it could be assumed that the PCC is in open circuit). Using this approximation, the damping coefficient produced by the virtual resistance R_v, is

$$\zeta = \frac{R_v}{2}\sqrt{\frac{C_f}{L_f}}. \tag{1}$$

Using (1), it is relatively simple to design a value of R_v which reduces the voltage oscillations produced by the undamped $L-C-L$ system located at the converter output. In this paper, R_v is designed to achieve a damping coefficient in the range of [0.3–0.4]. Notice that the active damping system affects the inner control system and has little effect in the active reactive power sharing between the generating units located in the four-leg microgrid.

The proportional controller K_p is designed to achieve a natural frequency, in the current control loop, of about 100 Hz. A 3-D space vector modulation (3-D SVM) algorithm is used to synthesize the voltage at the converter output [7]. The influence of the secondary control loops (see Section IV) in the calculation of the single-phase voltage v^*_{aj} is represented by the block labeled $f(u)$ in Fig. 2.

For the implementation of the control algorithms, single-phase PLLs are required. The PLLs are utilized to synchronize the power converters to the grid, for self-tuning of the PR controllers and for the implementation of secondary control algorithms (among other things). Because of simplicity, the single-phase PLLs are not shown in Fig. 1.

A. Single-Phase PLL and QSG

Single-phase PLLs are well known [25]–[27]. For completeness, a brief discussion is realized in this section. Because a QSG is relatively slow, the dynamic performance of this device has to be analyzed before designing the secondary control systems. To the best of our knowledge, the modeling and dynamic of a single-phase PLL based on a QSG have not been discussed previously and it is analyzed in this paper (see Section IV). The input of a typical PLL has two components that can be represented as a vector in α–β coordinates [27]. However, in a single-phase system, the β component is not available and has to be created

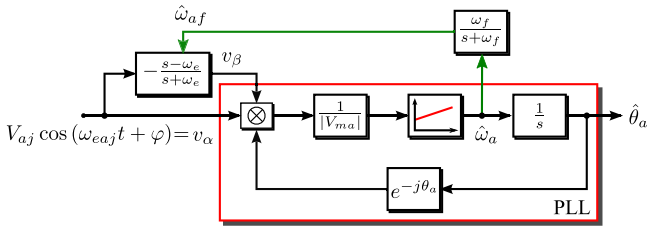

Fig. 3. Single-phase PLL based on an APF.

using a quadrature signal generator (or QSG). There are several QSG proposed in the literature and, in this paper, the all-pass filter (APF) has been selected mainly because of its implementation simplicity and good performance when the grid frequency variation is small respect to a center frequency ω_e^* (see [25] and [26]). Therefore, the transfer function of the QSG used in this paper is

$$G_{\text{apf}}(s) = -\frac{s-\omega_e}{s+\omega_e}. \tag{2}$$

As it is simple to demonstrate (see [25]), the APF acts as a quadrature signal generator (QSG) producing a phase shift of 90° when applied to a sinusoidal waveform of frequency ω_e. Furthermore, the gain of the APF is equal to unity for signals of this frequency (i.e., $|G_{\text{apf}}(s)| = 1$ for $s = j\omega_e$).

The single-phase PLL used in this paper is depicted in Fig. 3 (one PLL per phase is required). The symbol $\otimes$ represents the cross product between the vectors $\underline{v}_{aj}$ and the unitary vector $\widehat{\Theta}_a$; the term $1/|V_{ma}|$ is used to normalize the error at the output of the cross product and the estimated frequency $\widehat{\omega}_a$ is required to maintain the APF tuned. In the digital implementation, a low-pass filter (LPF) with a cutoff frequency ω_f could be required to eliminate the high-frequency noise from $\widehat{\omega}_a$.

The small signal dynamic model of a PLL is well known and reported in the literature [28]. However, the dynamic interaction between the QSG and the PLL has been hitherto unreported and it is addressed ahead in Section IV, "Secondary Control System."

B. Inner Control Loop

The control of the currents and voltages at the output of the four-leg power converter is realized using nested control loops to regulate each of the single-phase voltages. The external loop is based on proportional resonant (PR) controllers to track with zero steady-state error the sinusoidal voltage reference v_{aj}^* (see Fig. 2 and [29] and [30]). Because the electrical frequency of the system is varying, a self-tuning controller is required in this paper (see [7] and [30]) to maintain a good dynamic performance in the controller.

An internal current controller is used in Fig. 1. This faster internal control loop is required mainly to avoid overcurrent at the converter output. However, it is not necessary to provide zero steady-state tracking error in the current loop. Therefore, a proportional controller is implemented in this case.

The output of the converter is connected to a poorly damped *LCL* system, composed of a second-order (*LC*) power filter and a distribution line with a relatively small resistive component. Therefore, an active damping component based on a virtual programmable resistor is added to the proportional controller output. Using this methodology, the relatively large oscillations, typically produced in *LCL* systems, are mitigated or eliminated [24].

As depicted in Fig. 2, the output of the controller is synthesized using a 3D-SVM algorithm. Notice that the 3D-SVM reported in [7] can synthesize voltages of different magnitudes and frequencies in each of the single-phase outputs.

C. Droop Control Systems

When the load is unbalanced, the currents and voltages at the PCC may have components of positive, negative, and zero sequences. In this case, the conventional droop control algorithm can hardly achieve good sharing of the active and reactive power and there is no straightforward solution to cooperative sharing of imbalance between inverters. In this paper, a simple solution is proposed based on single-phase independent droop control. If single-phase voltages are independently regulated, in magnitudes as well as frequencies, the power to frequency (P–ω) droop control laws are defined for each phase as

$$\omega_{ij} = \omega_e^* - m_{\omega_{ij}}\,(P_{ij} - P_0) \tag{3}$$

where $i = a, b, c$ stands for the phase label and $j = 1, 2, 3\ldots$ is the converter number. The reference frequency ω_e^* is 50 Hz and P_0 is the center power [3], [20]. Notice that the P_{ij} powers of (3) have to be calculated for each phase of every four-leg converter located in the system. The single-phase instantaneous active power is initially calculated as

$$P_{ij}(t) = v_{ij}(t) \cdot i_{ij}(t). \tag{4}$$

The single-phase active powers from (4) are filtered using a self-tuned notch filter, in order to eliminate the $2\omega_e$ signal component from $P_{ij}(t)$. As usual, an LPF is also applied to the active power, to reduce the dynamic of the droop control algorithm avoiding cross coupling between the droop control and the voltage and current control loops of the power converters [3]. Notice that the implementation of the single-phase droop control algorithm proposed in this paper does not required to estimate the positive-, negative-, and zero-sequence components of the voltage and currents. Droop control to regulate the reactive power (Q–V droop) can be also applied to the four-leg system. In this case, the magnitude of each single-phase voltage is calculated using

$$V_{ij} = V^* - m_{\text{qij}} \cdot Q_{ij}. \tag{5}$$

The reactive power Q_{ij} is calculated using the quadrature voltage produced at the QSG output. Therefore, the reactive power is obtained as

$$Q_{ij}(t) = v_{\beta ij}(t) \cdot i_{ij}(t). \tag{6}$$

Again, the reactive power calculated from (6) is filtered out using a self-tuned notch filter and an LPF. The droop control systems, including self-tuned notch and LPFs, are shown in Fig. 4.

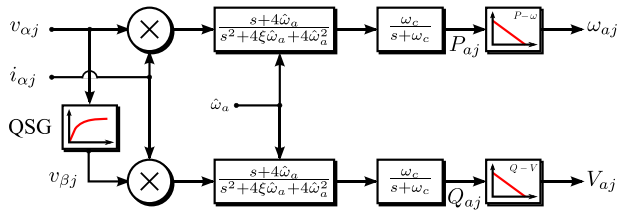

Fig. 4. Implementation of the single-phase droop control systems.

III. Analysis of the Effects Produced by Small Frequency Deviations in Each of the Phase-to-Neutral Voltages

As stated in Section I, the control system and microgrid topology proposed in this paper are more suitable for isolated grids in rural areas, where the load is of single-phase nature and power converters could be used to interface variable speed drives and other sort of frequency-sensitive three-phase loads that are required in the system. However, some equipment, as for instance power transformers, can operate adequately in the presence of short-time perturbations in the frequencies (see Section V). The effects of using phase-to-neutral voltages of different frequencies are analyzed in this section using a vector representation of the voltages at the PCC.

Assuming that the voltage in the load has little variation between phases, the phase-to-neutral voltages at the PCC can be obtained as

$$\begin{aligned} v_a &= V_m \cos(\omega_a t) \\ v_b &= V_m \cos(\omega_b t + 2\pi/3) \\ v_c &= V_m \cos(\omega_c t - 2\pi/3) \end{aligned} \tag{7}$$

where it is assumed that $\omega_a = \omega_e + \Delta\omega_a$, $\omega_b = \omega_e + \Delta\omega_b$, and $\omega_c = \omega_e + \Delta\omega_c$. Furthermore, the single-phase voltages can be obtained as

$$\begin{aligned} v_a &= 0.5V_m(e^{j\omega_a t} - e^{-j\omega_a t}) \\ v_b &= 0.5V_m(e^{j(\omega_b t+2\pi/3)} - e^{-j(\omega_b t+2\pi/3)}) \\ v_c &= 0.5V_m(e^{j(\omega_c t-2\pi/3)} - e^{-j(\omega_c t-2\pi/3)}). \end{aligned} \tag{8}$$

Using the standard vector representation of the single-phase voltages shown in (8) yields

$$\underline{v} = \frac{2}{3}\left(v_a + v_b e^{-j2\pi/3} + v_c e^{j2\pi/3}\right). \tag{9}$$

Replacing (8) in (9) and after some manipulations, the following is obtained:

$$\begin{aligned} \underline{v} = \frac{V_m}{3}e^{j\omega_e t}\left(e^{j\Delta\omega_a t} + e^{j\Delta\omega_b t} + e^{j\Delta\omega_c t}\right) + \frac{V_m}{3}e^{-j\omega_e t} \\ \times \left(e^{-j\Delta\omega_a t} + e^{-j(\Delta\omega_b t-2\pi/3)} + e^{-j(\Delta\omega_c t+2\pi/3)}\right). \end{aligned} \tag{10}$$

Therefore, the response is composed of a positive sequence component (i.e., the term containing $e^{j\omega_e t}$) and a negative sequence component (i.e., the term containing $e^{-j\omega_e t}$). The positive and negative components have phases and magnitudes that are a function of ($\Delta\omega_a$, $\Delta\omega_b$, $\Delta\omega_c$). When the frequencies deviations $\Delta\omega_x$ are driven to zero, then the voltage vector is equal to $\underline{v} = V_m e^{j\omega_e t}$, which represent a balanced voltage.

To drive the frequency deviations ($\Delta\omega_a$, $\Delta\omega_b$, $\Delta\omega_c$) to zero, secondary control systems are required, as discussed in the following section.

IV. Secondary Control Systems Proposed in This Paper

The secondary control systems proposed in this paper are designed to achieve a balanced voltage operation at the PCC. Therefore, in steady state, the single-phase voltages at the PCC have negligible zero/negative sequence components and are operating with a fixed 50 Hz frequency. For these tasks, three secondary control systems are proposed in this research effort. A secondary voltage amplitude control loop, a secondary frequency control loop, and a PCC voltage angle balancing control loop. The latter is designed to regulate a phase shift of $2\pi/3$ between the single-phase voltages.

A. Small Signal Model of the QSG

The dynamic of the QSGs has to be considered for the design of all the secondary control loops. To the best of our knowledge, small signal models of QSGs have hitherto been undiscussed in the literature.

As mentioned before, quadrature signal generators can be applied to create a fictitious rotating vector from a single phase to neutral voltage. In this paper, it is assumed that the beta component of the voltage is produced by the QSG, whereas the alpha component is the single phase to neutral voltage measured by the control system, for instance, $\underline{v}_a = v_a + jv_\beta$, where v_β is obtained by applying the APF of (2) to the single-phase instantaneous voltage v_a of (7). Using this methodology, it is simple and intuitive to conclude that the relatively slow dynamic of the QSG has to be considered when designing the secondary control systems and for adjusting the bandwidth of the PLLs required in the microgrids. For instance, if a perturbation is produced at the single-phase instantaneous voltage v_a, the perturbation is going to take a time to propagate to the v_β component of the fictitious rotating vector $\underline{v}_a$, and during this propagation period, the PLL is going to produce an incorrect estimation of the frequency and voltage angle of $\underline{v}_a$. Therefore, in this section, the dynamic of the QSG-based PLL is analyzed.

The single-phase voltage signal of phase a is defined as $v_a = V_{ma}\cos(\omega_{ea}t)$, which is defined as the alpha component of the fictitious rotating vector, or v_α. Considering that the single-phase voltage is subjected to small signal variations ΔV_m and $\Delta\Theta_{\text{gea}} = \Delta\omega_{ea}t$ (corresponding to perturbations in the magnitude and frequency, respectively, of the voltage v_a at the PCC side), it is possible to analyze the effect of this perturbation in the fictitious rotating vector $\underline{v}_a$ considering the variation in Δv_α and Δv_β, respectively. Therefore,

$$\begin{aligned} \Delta v_\alpha &= \frac{\partial v_\alpha}{\partial V_m}\Delta V_m + \frac{\partial v_\alpha}{\partial \Theta_{\text{gea}}}\Delta\Theta_{\text{gea}} \\ &= \Delta V_m \cos(\omega_{ea}t) - \Delta\Theta_{\text{gea}} V_m \sin(\omega_{ea}t). \end{aligned} \tag{11}$$

Using the Laplace transform , $\Delta v_\alpha(s)$ is obtained as

$$\Delta v_\alpha(s) = \Delta V_m \frac{s}{s^2+\omega_{ea}^2} - \Delta\Theta_{\text{gea}} V_{m0} \frac{\omega_{ea}}{s^2+\omega_{ea}^2}. \tag{12}$$

Meanwhile, to obtain the value of Δv_β, the dynamic of the APF given by (2) has to be considered

$$\Delta v_\beta(s) = -\Delta v_\alpha(s) \frac{s-\omega_{ea}}{s+\omega_{ea}}. \tag{13}$$

Replacing (12) in (13), and using the inverse Laplace transform, we obtain

$$\begin{aligned}\Delta v_\beta = {} & \Delta V_m[\sin(\omega_{ea0}t) - e^{-\omega_{ea0}t}] \\ & + \Delta\Theta_{\text{gea}} V_{m0}[\cos(\omega_{ea0}t) - e^{-\omega_{ea0}t}].\end{aligned} \tag{14}$$

Therefore, after a perturbation in magnitude and/or frequency is applied to the voltage v_{an}, the fictitious voltage $\underline{v}_a$ will be affected (in the beta components) by the transient terms $e^{-\omega_{ea0}t}$. For a 50-Hz grid, the term $e^{-\omega_{ea0}t}$ is approximately negligible after 16 ms ($t \approx 5/\omega_{ea}$). However, during the transient, the voltage angle of $\underline{v}_a$, given by $\Theta_a = \tan^{-1}(v_\beta/v_\alpha)$ is incorrect until steady state is achieved at the QSG output. The error produced by the transient terms $e^{-\omega_{ea0}t}$ in the voltage angle at the input of the PLLL (Θ_a) could be calculated using a small signal model derived around a quiescent point $v_{\alpha 0}$, $v_{\beta 0}$

$$\Theta_a = \tan^{-1}(v_\beta/v_\alpha) \rightarrow \Delta\Theta_a = \frac{\partial\Theta_a}{\partial v_\alpha}\Delta v_\alpha + \frac{\partial\Theta_a}{\partial v_\beta}\Delta v_\beta. \tag{15}$$

Notice that Θ_{ge} is the angle at the grid side and Θ_a is the angle at the PLL input. Using (15) and the differentiation of the $\tan^{-1}$ function yields

$$\Delta\Theta_a = \frac{V_{\alpha 0}}{V_{\alpha 0}^2+V_{\beta 0}^2}\Delta v_\beta - \frac{V_{\beta 0}}{V_{\alpha 0}^2+V_{\beta 0}^2}\Delta v_\alpha. \tag{16}$$

Considering (11) and (14) and replacing them in (16), the variation $\Delta\Theta_a$ is calculated as

$$\Delta\Theta_a \approx \Delta\Theta_{\text{gea}} - e^{-\omega_{ea0}t}\cos(\Theta_{\text{gea0}})\left[\frac{\Delta V_{ma}}{V_{ma0}} + \Delta\Theta_{\text{gea}}\right] \tag{17}$$

Therefore, the angle at the input of the PLL is affected by a term proportional to $e^{-\omega_{ea0}t}$. This term is maximum when the perturbation is produced at $\Theta_{gea0} = 0$ (i.e., when v_α is maximum). Hence, after a disturbance in the grid, the angle at the PLL input will be affected by the exponential terms $e^{-\omega_{ea0}t}$ for less than 16 ms (considering 50-Hz operation).

Considering the small signal model of a PLL, previously reported in [28], the model of the whole system PLL-QSG is depicted in Fig. 5. Notice that the angle estimated by the PLL corresponds to $\widehat{\Theta}_a$, whereas the frequency estimated by the PLL algorithm is $\widehat{\omega}_{ea}$.

B. Secondary Control System for Frequency Regulation

The proposed secondary control system for frequency regulation at the PCC is shown in Fig. 6. Three control systems (one per phase) are required. The frequencies are estimated by the single-phase PLLs at the PCC and then compared with the reference frequency ω_e^*. The error is processed by a PI controller to achieve zero error in steady-state conditions. The controller output is $\Delta\omega_{sf_i}$ where the subscript "sf" stands for secondary control of frequency and $i = a, b, c$ identify the phase whose frequency is being regulated. Notice that the term $\Delta\omega_{sf_i}$, at the PI controller output, is added to the frequency control (of phase "*i*") in all the power converters of the system. The terms ω_{Ta}, ω_{Tb}, and ω_{Tc} represent the contributions of other control loops (e.g., droop control) to the frequency regulation. However, for the design of the $\Delta\omega_{sf_i}$ frequency control loops, ω_{Ta}, ω_{Tb}, and ω_{Tc} are external perturbations and their effects could be neglected.

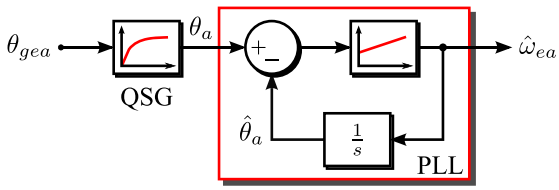

Fig. 5. Linearized PLL and QSG system.

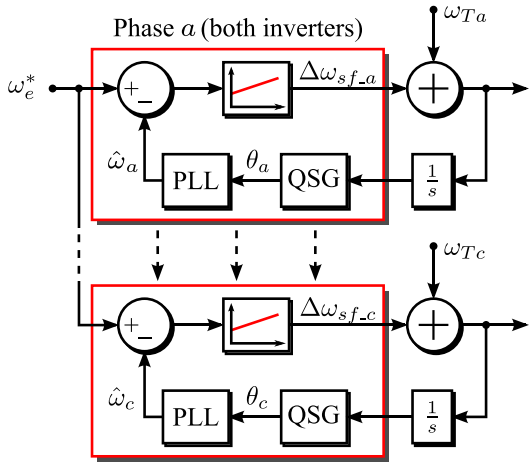

Fig. 6. Secondary control system for the nominal frequency restoration.

In this paper, the PI controller required to calculate $\Delta\omega_{sf_i}$ (see Fig. 6) is designed to achieve a closed-loop bandwidth of $\approx$ 1 Hz and the single-phase PLL is designed for a closed-loop bandwidth of about $\approx$ 10–15 Hz, corresponding to a settling time of $t_s \approx$ 55–80 ms. With this relatively low bandwidth, the effects introduced by QSG dynamics can be neglected, because the QSG settling time is 3.5 to 5 times faster than that corresponding to the single-phase PLL. Notice that the control system for the regulation of the frequencies in the single-phase voltages are based on PI controllers. Therefore, according to the internal model principle (see [7], and [9]), zero error in steady state is achieved.

C. Angle-Balancing Secondary Control System

When the frequency is restored, the three phases at the PCC are operating at 50 Hz. However, because of the P–ω per-phase

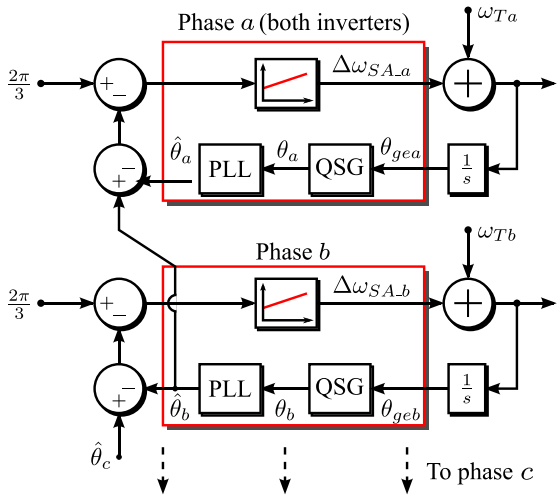

Fig. 7. Angle-balancing secondary control system.

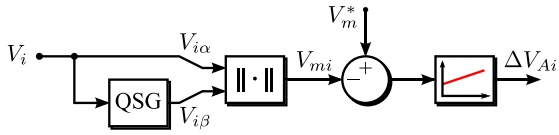

Fig. 8. Secondary control system for voltage regulation at the PCC.

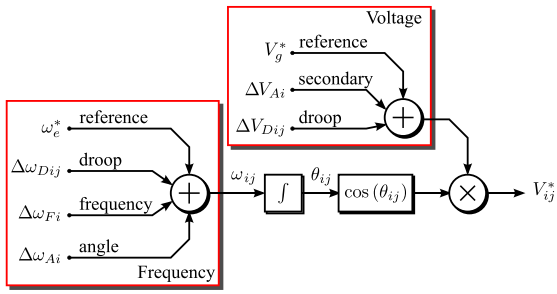

Fig. 9. Generation of the reference voltage signal for each phase $i = a, b, c$ and each converter $j = 1, 2, 3 \ldots$.

droop control, the phases could be operating with unbalanced phase shifts, (e.g., phase shifts $\neq 2\pi/3$ rads between consecutive single-phase voltages). This may pose several problems, for instance, a relatively large current component circulating in the neutral wire, even if the load is balanced. Moreover, because the phase shifts between voltages at the PCC are unbalanced, there are negative- and zero-sequence components in the load voltage and this may produce some negative effects in the power quality.

To avoid the aforementioned drawbacks, the angle-balancing secondary control system shown in Fig. 7 is proposed. The system operates by measuring the angle of each voltage at the PCC side. Three PI controllers are used to drive the angle difference between the phase voltages to 120°. To avoid dynamic couplings between the secondary frequency control system and the angle-balancing control system discussed in this section, the latter should be designed with a slower bandwidth.

As shown in Fig. 7, the output of the proposed secondary control system is $\Delta\omega_{SA_i}$, where the subscript "SA" stands for the angle-balancing secondary control. This signal is transmitted to each of the power converter in phase "*i*." As discussed in Section VI, the proposed angle-balancing control system is able to balance effectively the voltages at the PCC. However, this is achieved by unbalancing the voltages at the output of the converters. In this paper, it is assumed that the load is connected at the PCC side.

The PI controller required to calculate $\Delta\omega_{SA_i}$ (see Fig. 7) is designed to achieve a closed-loop bandwidth of $\approx$0.5 Hz, i.e., about half the dynamic of the secondary control system for the frequency. With this simple design, most of the cross couplings between both secondary control systems are avoided.

D. Secondary Control to Regulate the Phase-Voltage Magnitudes

Three voltage control loops are used to regulate the voltage magnitude at the PCC. Again, the proposed control system is centralized and the voltage signal ΔV_{Ai} is transmitted to adjust the voltage in the phase "*i*" of each of the power converters (see Fig. 8).

Notice that the voltage magnitude V_{mi} is calculated considering the quadrature signal generator proposed in this paper.

The secondary control for the voltage is designed to achieve a closed-loop bandwidth of about 1.0 Hz. Again, most of the cross couplings with the other two secondary control systems are avoided using this relatively low bandwidth.

E. Overall Frequency and Voltage Control System

The contributions of all the secondary control systems presented in this section are used in each of the converters of the microgrid to regulate the frequencies and magnitudes of the phase-to-neutral voltages. This is further explained in Fig. 9.

The label "droop" in Fig. 9 corresponds to the frequency and voltage variations calculated using (3) and (5), respectively. The voltage signal ΔV_{Aij} is calculated using the control system depicted in Fig. 8. Finally, the signals $\Delta\omega_{Fi}$ and $\Delta\omega_{Ai}$ are produced by the secondary control systems of frequency and angle balancing, respectively (see Figs. 6 and 7). Notice that the block labeled "*f(u)*" in Fig. 2 is explained using Fig. 9.

V. Simulation Work

The performance of the proposed control system has been compared with that obtained utilizing two well-known strategies reported in the literature for collaborative control of power converters operating in three-leg/four-leg microgrids [8], [20]. These are as follows.

1) The conventional P–ω droop control strategy (see [20]) that regulates the output frequency of the converter "i" using the expression

$$\omega_i = \omega_e^* - m_{pi}\left(P_i - P_0\right) \tag{18}$$

where ω_i is obtained considering the total converter output power P_i. Notice that in (18), the frequencies of all the

TABLE I
CONTROL SYSTEM PARAMETERS

Description	Symbol	Value
Active damping virtual resistor	R_v	$\approx 2.0\ \Omega$
Voltage controller (inner control loop)	ω_v	40-45 Hz
LPF droop (primary control loop)	ω_C	5.0 Hz
Frequency secondary control loop	ω_{n1}	1.0-1.2 Hz
Angle secondary control loop	ω_{n2}	0.5-0.7 Hz
Voltage secondary control loop	ω_{n3}	1.2-1.5 Hz
Natural frequency of the PLLs	ω_{PLL}	15-20 Hz
Notch filter broadband	$\mathbf{BW}_N$	$\approx$ 1.0 Hz
SP-PLL frequency tuning (see Fig. 3)	ω_f	10.0 Hz

TABLE II
EXPERIMENTAL SYSTEM PARAMETERS

Description	Symbol	Value
Switching frequency	f_{SW}	$\approx$7140 Hz
Switching period	T_{SW}	140 μS
dc-link capacitor	C_{dc}	1650 μF
LC filter capacitor	C_f	40/45 μF
LC filter inductor	L_f	2.5 mH
Line inductor	L_l	5.0/2.5 mH
Converter Nom. Power	P_n	3.0 kW

phases at the output of a given converter are regulated to the same value. This is different to the proposed control method where the phase frequencies are independently regulated using (3).

To regulate the magnitude of the converter's output voltage, a conventional Q–V droop control strategy is used

$$V_i = V^* - m_{qi}\,(Q_i - Q_0) \tag{19}$$

where V_i is obtained considering the total converter reactive power Q_i. Again, (19) is different to the proposed methodology where in each converter, the phase-to-neutral voltage could be regulated to different magnitudes using (5).

2) The control system proposed in [8] where collaborative control of four-leg converters is discussed. The imbalances are shared considering negative- and zero-sequence virtual—impedance loops that are used to add negative- and zero-sequence components to the voltages synthesized by each converter in the microgrid. The methodology suggested in [8] has been used in this paper to calculate the virtual impedances.

Notice that in all the works where the utilization of virtual impedance loop is proposed, e.g., [8], [9], [12]–[14], and [22], the frequencies of all the phases, at the output of a given converter, are regulated to the same value.

The performance of the two control strategies discussed before (i.e., those reported in [8] and [20]), as well as the performance of the control systems proposed in this paper have been compared using computer models implemented in the simulation software PLECS, considering the microgrid topology depicted in Fig. 1 and, unless otherwise stated, the parameters of Tables I and II. The performance of the control strategies have been compared considering two goodness factors, which are as follows. First, single-phase and three-phase (total) power sharing between the converters. Second, imbalances in the voltage supplied at the PCC. This imbalance is measured considering the deviations in the magnitudes and angular phases of the voltages [see (20) and (21)].

To test the performance of the three control strategies for sharing active power, a resistive balanced load of 5 kW(1.66-kW per phase) is initially connected at the PCC. At $t = 2$ s, the load is unbalanced by disconnecting 1 kW from phases a and b, respectively. Therefore, after the step change, the total load is reduced from 5 to 3 kW. To consider a more general scenario, it is assumed that the inductances connecting the converters at the PCC could have different values (e.g., $L = 5$ mH and $L = 2$ mH).

The dynamic and steady-state performances of the three control strategies are shown in Fig. 10. In $t = 2$ s, the load connected at the PCC, in phases a and b, is changed from 1666 to 666 W (in each phase). For the three control strategies, the powers supplied by converters 1 and 2 are shown using blue and red lines, respectively. Notice that in all the cases, the total power is equally shared by both the converters. However, only the proposed control strategy is able to effectively share the single-phase powers. Moreover, as reported in the literature [10], when virtual impedances are used, the sharing of the powers is strongly affected by the impedances of the lines connecting the converters to the PCC. Nevertheless, the methodology proposed in this paper achieves good power sharing (single-phase and total power) even if the line inductances are not similar.

The steady-state results corresponding to the test of Fig. 10 are shown in Fig. 11. Notice that the worst results in terms of single-phase power sharing are achieved by the conventional droop technique, where inverter 1 supplies 63% of the power connected at the PCC in phase b, and inverter 2 supplies 58.2% of the power connected in phase c. The best performance in terms of power sharing is achieved by the proposed control strategy, followed by the strategy based on virtual impedances. The control strategy proposed in this paper is the only one able to equally share the single-phase powers and three-phase power, in both converters.

To measure the voltages imbalances at the PCC, two expression are used. First at all, the phase voltage unbalance rate (PVUR [10]) is defined as

$$\text{PVUR} = \frac{\text{Max}|(V_i - V^*)|}{V^*} \tag{20}$$

where V^* is the nominal PCC voltage, and $i = a, b, c$. Second, the phase difference rate (PD) is defined as

$$\text{PD} = \frac{\text{Max}|\delta_{ij} - \frac{2\pi}{3}|}{\frac{2\pi}{3}} \tag{21}$$

where δ_{ij} is the phase angle between the voltages (V_i, V_j) and $ij = ab, bc, ca$. As shown in Fig. 12, the method based on virtual impedance produces a higher PVUR value, but less deviation in the angular phases. On the other hand, the conventional droop control produces a relatively high deviations in the angular phase. For the proposed control methodology, the secondary control systems for the regulations of the angular phase differences (see Fig. 7) and for the regulation of the single-phase

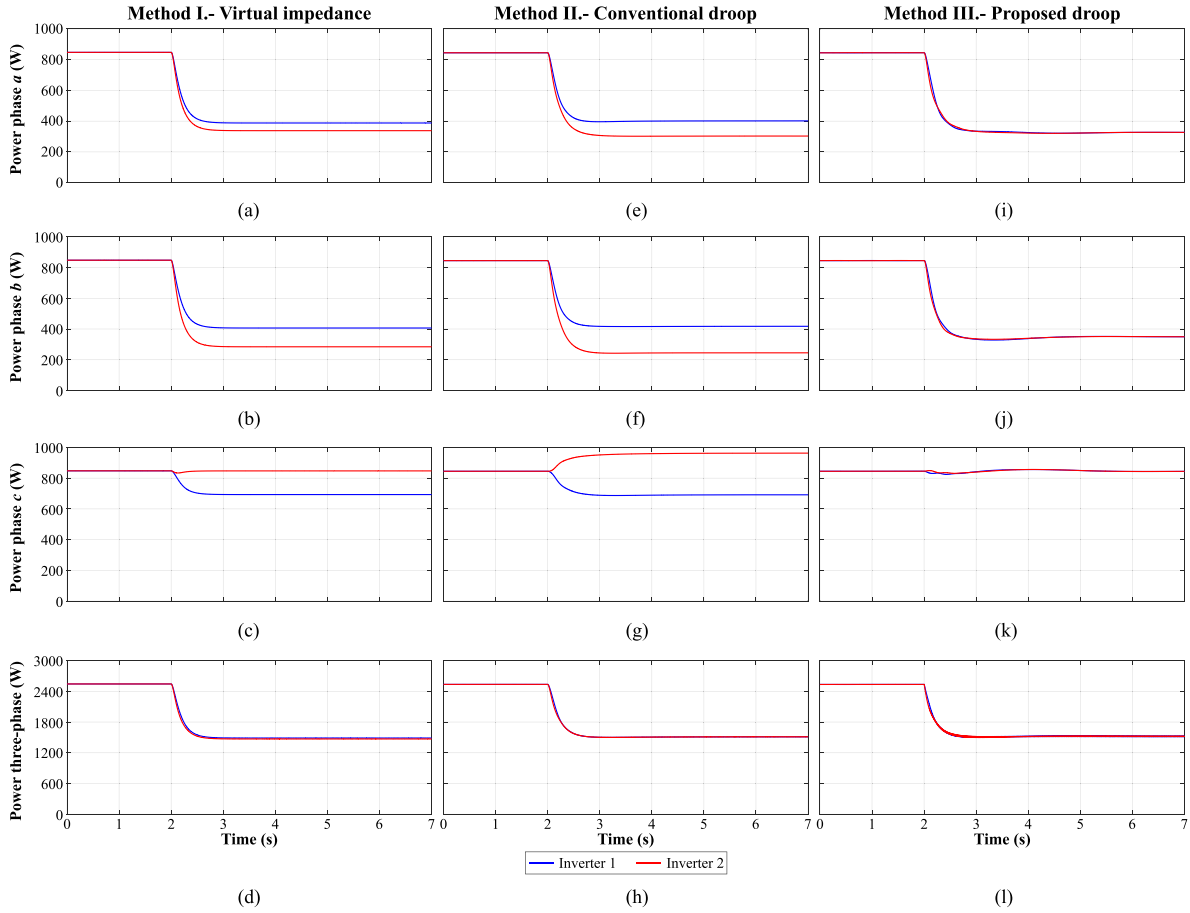

Fig. 10. Performance of the three control strategies compared.

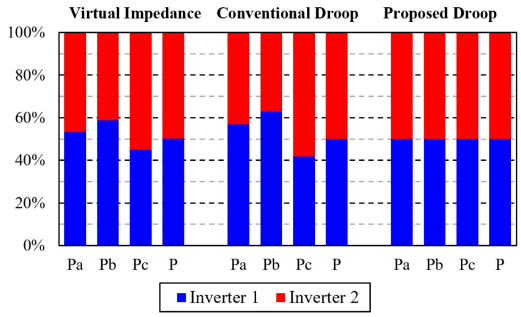

Fig. 11. Steady-state results corresponding to the previous test.

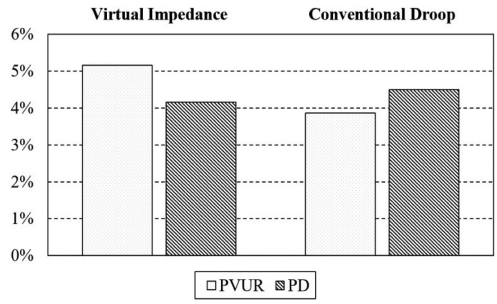

	PVUR	PD	In1	In2
Virtual impedance	5,2%	4,2%	31,2%	68,8%
Conventional droop	3,9%	4,5%	28,6%	71,4%
Proposed droop	0,0%	0,0%	38,4%	61,6%

Fig. 12. PVUR and PD corresponding to the previous test. These values are calculated at the PCC.

voltage, magnitudes (see Fig. 8) ensure that the values of PVUR and PD are ≈ 0 in steady state. Notice that the total load neutral current is also shared more evenly for the proposed control system (see Fig. 12).

A. Sharing of the Reactive Power Using the Proposed Methodology

The performance of the proposed control system for sharing reactive power, when an unbalanced four-leg reactive load is connected at the PCC, is also studied in this paper. The load is initially composed of a 3-kW balanced resistor bank. In $t = 2$ s, a step change is applied, and the load in phases a and b are both changed to $P_{a,b} = 402$ W and $Q_{a,b} = 920$VAR (i.e., P.F= 0.4 lagging). The load connected to phase c is maintained in $P_c = 1000$ W during the whole test.

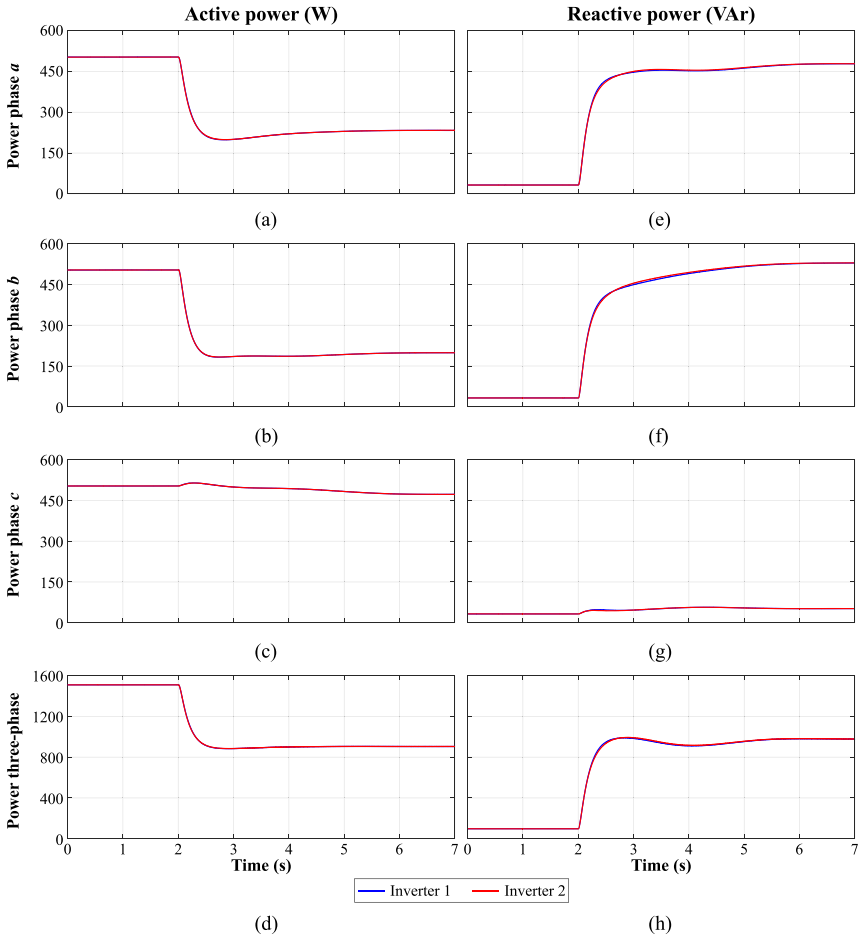

Fig. 13. Performance of the proposed control strategies for an unbalanced reactive power step.

The performance of the proposed control strategy is shown in Fig. 13. After $t = 2$ s, the proposed single-phase droop control changes the active and reactive power supplied by each leg of the power converters in order to achieve collaborative sharing. As shown in Fig. 13, the control strategy proposed in this paper is able to almost equally share the single-phase reactive powers and three-phase reactive power, in both converters.

B. Performance of the Proposed Control System Feeding a Three-Phase Transformer

As stated in Section I, the proposed collaborative control system for four-leg unbalanced microgrid has been proposed for the operation of rural microgrids. According to the experience of the authors, at least in developing countries, the load connected to these microgrids is composed of several single-phase loads (typically households) connected to different phases of the four-leg three-phase system (see [21]), with the electricity being used for heating, lighting, and single-phase home appliances. However, as demonstrated in this section, step-up and/or step-down power transformers could be also connected to variable frequency microgrids.

Therefore, in this section, the performance of the proposed collaborative control system feeding a delta-star three-phase transformer is simulated. The voltages and frequencies at the PCC for the experimental test, whose results are depicted in Fig. 18, have been utilized to simulate the performance of the transformer being fed by single-phase voltages of slightly different frequencies, with the results being shown in Fig. 14. For this test, it is assumed that the secondary of the transformer is feeding a star-connected $10\,\Omega$ resistive load. As discussed before, the biphasic load step is applied to the microgrid (primary of the transformer) at the PCC in $t \approx 3.5$ s and disconnected in $t \approx 11.35$ s, respectively (see Fig. 19). The input (primary) currents and voltages have variations of less than 15% [see Figs. 14(a) and (c)] in the RMS magnitudes. The instantaneous primary current is shown in Fig. 14(b) with a reduced imbalance produced by the negative sequence current circulating in the primary. Finally, Fig. 14(d) shows the secondary voltage that is well regulated with a reduced dip and overshoot.

VI. Experimental Work

The control strategies reported in this paper have been implemented in the experimental system shown in Fig. 15. Two 3-kW four-leg power converters designed in the power electronic lab at the University of Chile have been implemented. The system is controlled using DSK6713 Texas Instrument DSPs augmented

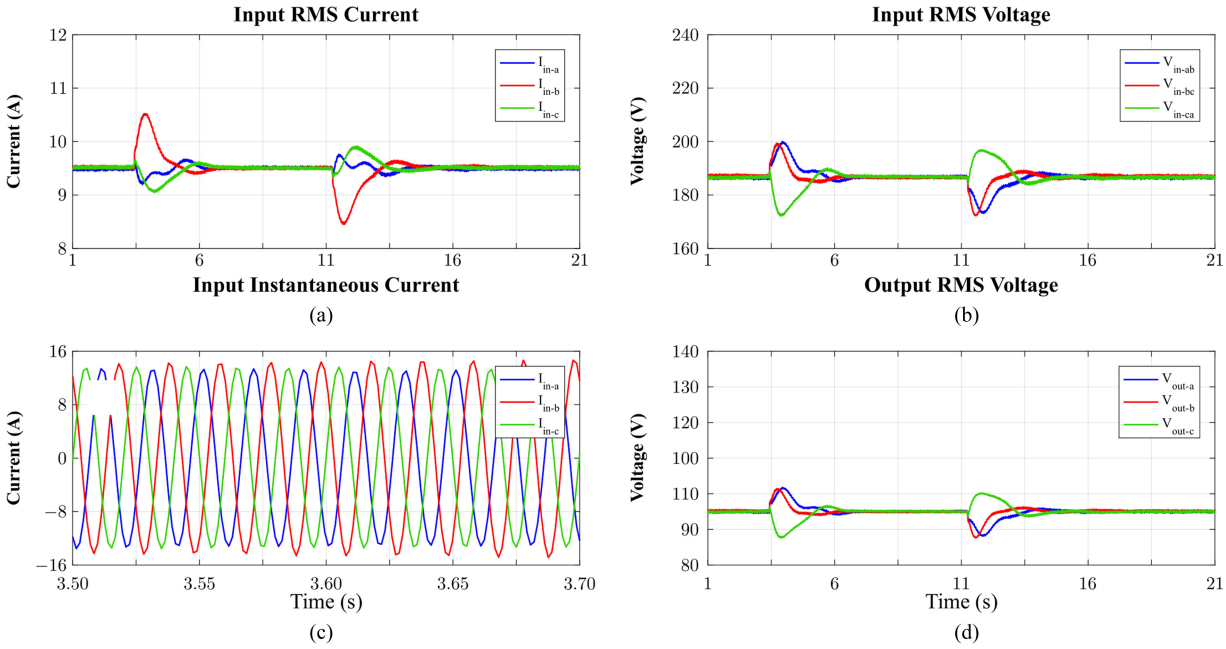

Fig. 14. Performance of the proposed control system feeding a delta-star transformer considering the experimental results presented in Fig. 18. (a) Primary current. (b) Primary rms voltages. (c) Secondary rms voltages. (d) Instantaneous primary current.

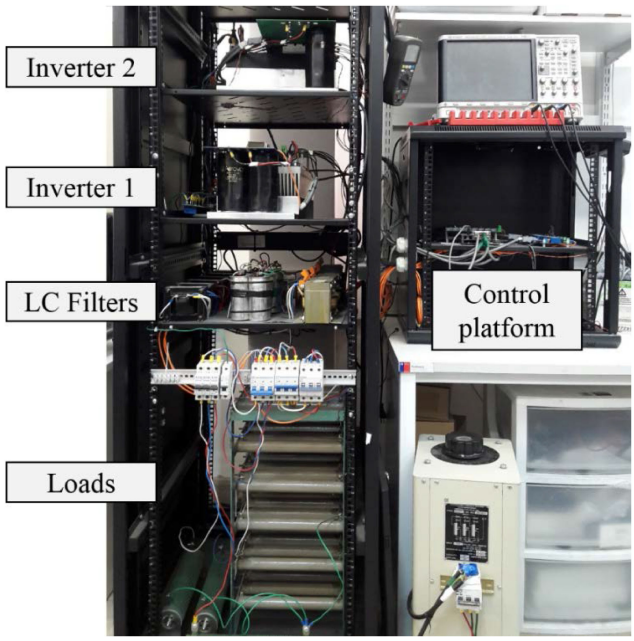

Fig. 15. Experimental three-phase four-wire microgrid used to validate this work.

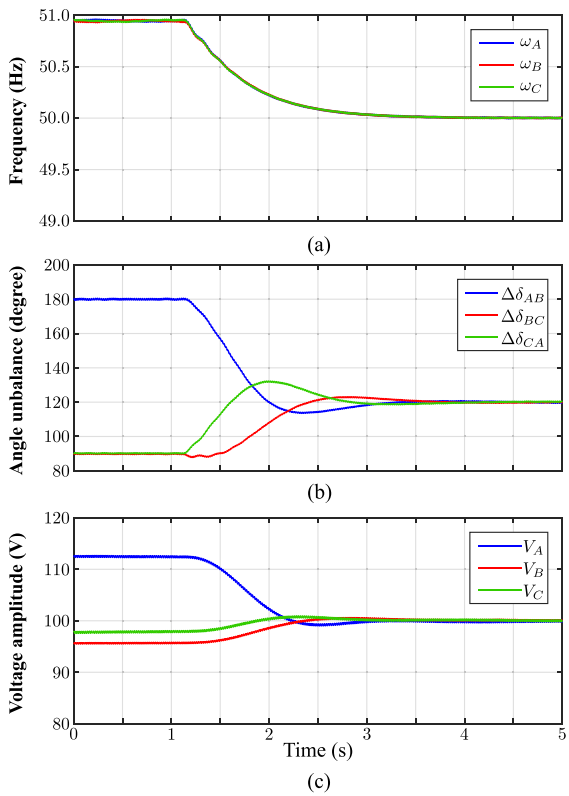

Fig. 16. Response of the secondary control systems. (a) Frequency. (b) Phase shift. (c) Voltage amplitude.

with FPGA boards that are required to handle the AD converters and for the implementation of the 3-D space vector modulations algorithms used with the four-leg converters. Hall effects transducers have been utilized to measure the currents and voltages at the converters output and at the PCC. The sampling time used is 140 μs, corresponding to a switching frequency of $\approx$ 7.14 kHz. More information about the parameters of the experimental system as well as the implementation of the primary and secondary control systems are depicted in Tables I and II.

The performance of the proposed secondary control systems is shown in Fig. 16 considering a star-connected resistive load of $\approx 20\ \Omega$ per phase. To test the performance of the secondary control systems operating in a worst case scenario, the condition

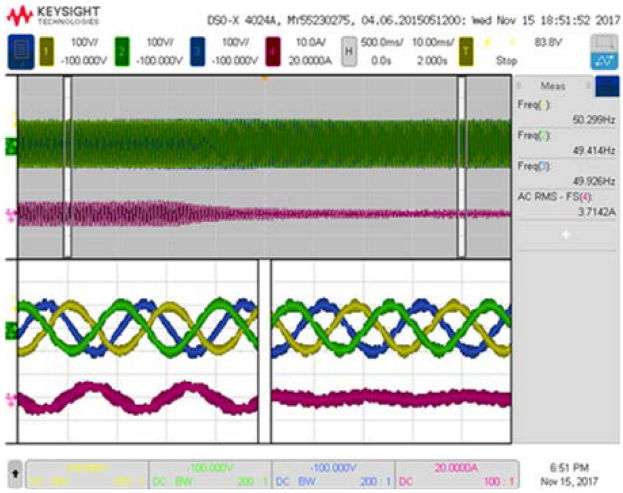

Fig. 17. Digital scope waveforms corresponding to the test of Fig. 16.

shown in Fig. 16(a) (for $t < 1$ s) has been selected. Therefore, before enabling the control systems, the microgrid in steady state is operating at $\approx$ 51 Hz (in all the phases) with a relatively large deviations in the voltage amplitudes and phase shifts of the single-phase voltages at the PCC. In $t \approx 1.167$ s, the three secondary control systems are enabled and all the frequencies are driven to 50 Hz [see Fig. 16(a)]. The phase shift between voltages (i.e., $\Delta\delta_{ca}$, $\Delta\delta_{bc}$, and $\Delta\delta_{ab}$) are driven to 120° degrees [see Fig. 16(b)] and the voltage amplitudes are driven to $\approx$ 100 V [see Fig. 16(c)]. The secondary control systems of the voltages and frequencies have similar settling times of ≈ 1.2 s. As discussed in Section III, the angle balancing control system is slower and takes about 2.0 s for the phase shifts to converge to 120°.

The waveforms captured by a digital scope (corresponding to the test of Fig. 16) are presented in Fig. 17. In this graphic, the three-phase-to-neutral voltage waveforms at the PCC are shown in green at the top graphic for the whole duration of the test.

Before enabling the secondary control systems, the voltages of phases *a* and *b* have a phase shift of about 180° (see bottom left of Fig. 17 corresponding to an amplified view of the highlighted area at the top left-hand side), which is corrected after enabling the angle balancing secondary control system. The balanced waveforms in steady state are shown at the bottom right-hand side of Fig. 17, and this corresponds to an amplified view of the highlighted area shown at the top right-hand side of Fig. 17.

In purple is shown the current circulating in the neutral of the load connected at the PCC. When the voltage phase shifts are incorrect (see left-hand side of Fig. 17), the neutral current is relatively large (see purple waveform) and this is corrected after the voltages are balanced in phase shift and magnitude (see right-hand side of Fig. 17).

Fig. 18 shows the system operating with a slightly unbalanced three-phase load of about 5 kW shared between both converters. The droop slopes are identical for each converter, therefore, each of them is supplying a three-phase power of $\approx$2.5 kW. A biphasic load step of about 1 kW is connected/disconnected between phases *a* and *b* of the PCC at $t \approx 3.5$ s and $t \approx 11.35$ s, respectively.

Fig. 18(a)–(c) shows the power supplied by both converters in phases *a*–*c*, respectively. At $t \approx 3.5$ s, the load between the two phases is disconnected and in $t \approx 11.35$ s, the load is connected again. From the experimental results, it is concluded that the droop control algorithm achieves good sharing of the single-phase active power connected at the PCC. Notice that the power supplied by phase *c* is barely affected by the load step at the PCC. As stated in Section I, virtually perfect sharing of the power consumed by the unbalanced load connected at the PCC is achieved with the simplified control strategy proposed in this paper. Only droop control algorithms and the proposed secondary control strategies have been required.

In Fig. 18(d), the experimental results for the frequency variations in all the phases are shown. After the load disconnection, the maximum frequency in one of the phases reaches 50.125 Hz and the secondary control system takes about 1 s to drive all the frequencies to 50 Hz. During this time, the frequencies of the voltages are slightly different (less than 0.1 Hz). The performance of the secondary control system regulating the phase shifts is shown in Fig. 18(e). As shown in this graphic, the phase shifts of the PCC voltages are driven back to 120° in ≈ 2.7 s. Notice that the maximum phase shift deviation corresponds to $\approx \pm 15°$ in the angle $\Delta\delta_{ca}$. Finally, the response of the secondary control system for voltage regulation is shown in Fig. 18(f). The peak deviation from the reference value is 7.5 V ($\approx 4.8\%$) and the disturbance is controlled in less than 2.4 s.

The performance of the proposed control system is also shown for a single-phase load step in phase *a*, but considering that the droop slope in the first inverter is twice the value of that used in the second converter. The experimental results are shown in Fig. 19. Notice that in all the tests, converter 1 supplies approximately twice the active power of converter 2 (the total load connected to the PCC is $\approx$ 3 kW). In $t \approx 3.3$ s, a single-phase load impact of 650 W is disconnected from phase *a* at the PCC and both power converters reduce the power supplied by phase *a* accordingly. Note that the active power supplied by the other two phases in both converters [see Fig. 19(b) and (c)] are barely affected by this load step.

Fig. 19(d) shows the variation in the load frequency, which is almost negligible in this case. Fig. 19(e) and (f) shows the response of the secondary control systems for regulating the phase shifts and voltage magnitudes, respectively. As depicted in these figures, the settling times are $\approx$2.6 s for the regulation of the single-phase voltage phase shifts and 1.9 s for the regulation of the single-phase voltage magnitudes.

Finally, the waveforms corresponding to the single-phase droop operation are shown in Fig. 20, for one of the converters. Notice that the single-phase voltage is well regulated with little distortion (see top waveform). This shows that the assumption that each phase-to-neutral voltage could be independently regulated is experimentally demonstrated correct. After the load disconnection, the currents (middle waveform) is reduced accordingly. Notice the double frequency oscillations shown in

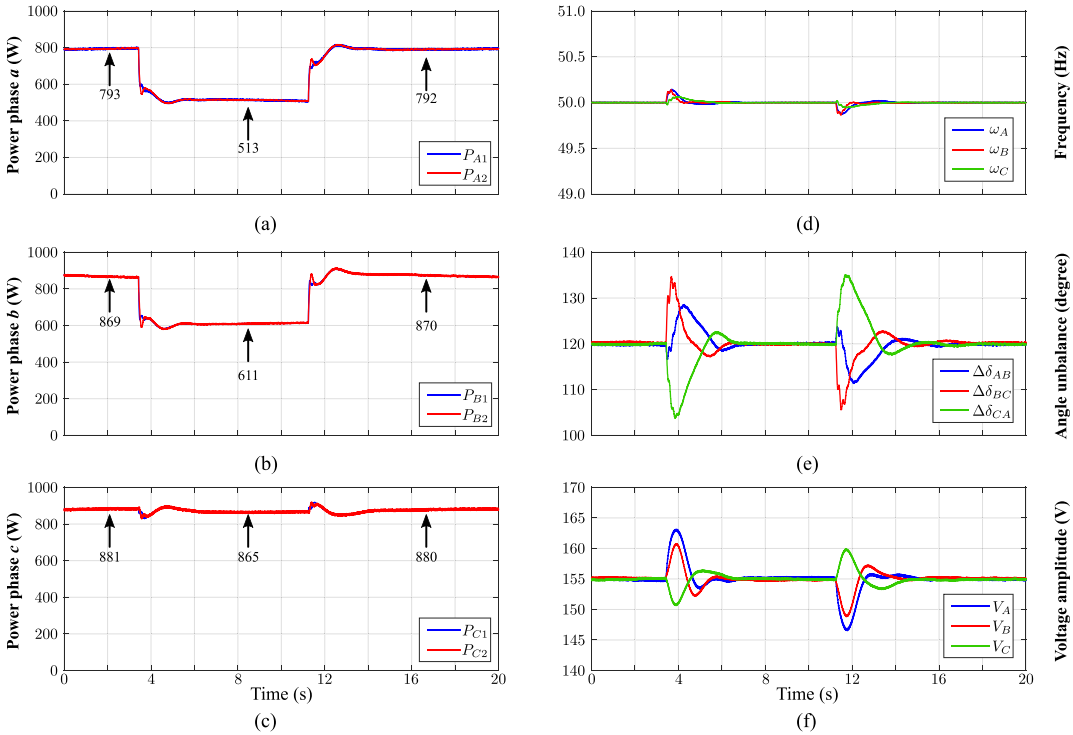

Fig. 18. Performance of the proposed control system considering the connection and disconnection of a 1-kW load between phases *a* and *b*. (a) Power in phase *a*. (b) Power in phase *b*. (c) Power in phase *c*. (d) Frequency measured at the PCC. (e) Phase shifts between single-phase voltages measured at the PCC. (f) Magnitude of the single-phase voltages at the PCC.

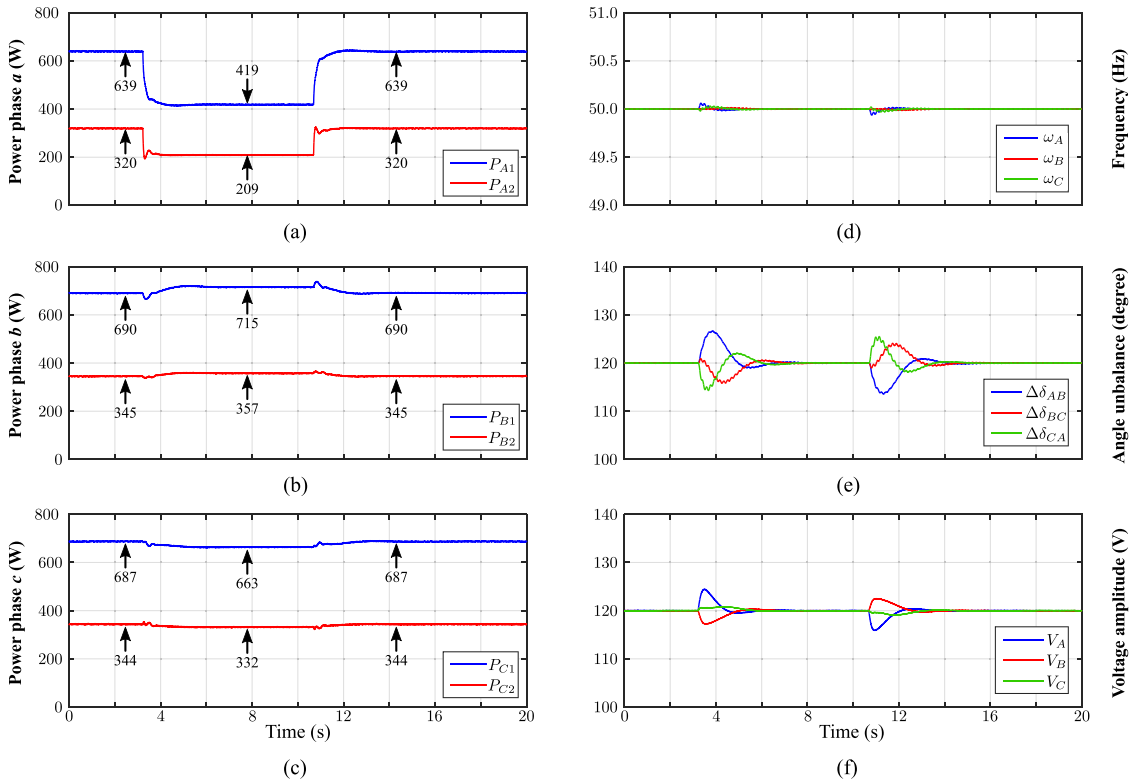

Fig. 19. Performance of the proposed control system considering the connection and disconnection of a single-phase load in phase *a*. (a) Power in phase *a*. (b) Power in phase *b*. (c) Power in phase *c*. (d) Frequency measured at the PCC. (e) Phase shifts between single-phase voltages measured at the PCC. (f) Magnitude of the single-phase voltages at the PCC.

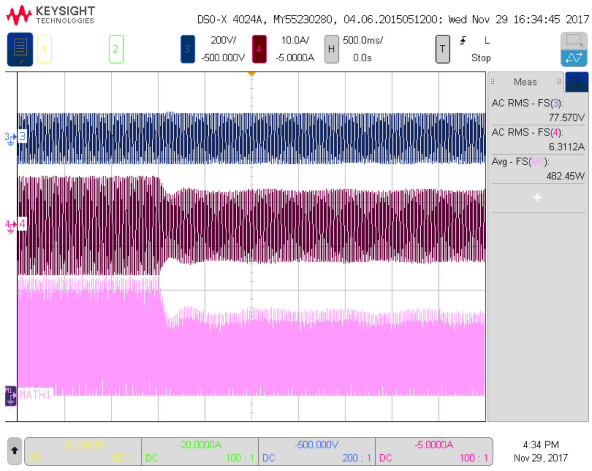

Fig. 20. Voltage, current, and instantaneous power for phase *a*, converter 1. Top waveform is voltage. Middle graph is currents and the bottom waveform is the instantaneous power.

the single phase power (bottom waveform), which are eliminated using the methodology depicted in Fig. 4.

VII. Conclusion

In this paper, a new control system to achieve collaborative power sharing in unbalanced three-phase four-wire microgrids has been presented. The proposed method is based on single-phase droop control augmented by three secondary control systems. Utilizing this simple methodology, the power produced by the positive-, negative-, and zero-sequence components of the voltages and currents at the PCC is effectively shared between the converters. Using the primary and secondary control systems discussed in this paper, it has been experimentally shown that in steady state, the voltages at the PCC are well regulated in amplitude and balanced, i.e., with negligible negative- and zero-sequence components. The proposed collaborative control system is suitable for single-phase loads and three-phase loads, which can tolerate relatively fast transient operation where the single-phase frequencies at the PCC are different between each phase. This is the case, for instance, of several small villages (isolated from the main grid) located in Patagonia Chile where the electrical consumption is based on single-phase loads (mainly residential loads) connected to the PCC.

The main advantage of the proposed methodology is implementation simplicity. Virtually perfect power-sharing control is achieved without requiring estimation of the positive-, negative-, and zero-sequence components of the voltage and current at the PCC. The utilization and tuning of virtual impedances is neither required for this implementation.

The proposed control system has been validated using a 5-kW experimental system composed of two four-leg power converters connected to the PCC using second-order power filters and transmission lines. The dynamic and steady-state performance of the system has been tested considering single-phase and biphasic load steps. In all the cases, the performance of the system has been excellent.

References

[1] R. Palma-Behnke *et al.*, "A microgrid energy management system based on the rolling horizon strategy," *IEEE Trans. Smart Grid*, vol. 4, no. 2, pp. 996–1006, Jun. 2013.

[2] D. Saez, F. Avila, D. Olivares, C. Canizares, and L. Marin, "Fuzzy prediction interval models for forecasting renewable resources and loads in microgrids," *IEEE Trans. Smart Grid*, vol. 6, no. 2, pp. 548–556, Mar. 2015.

[3] C. Ahumada, R. Cardenas, D. Saez, and J. M. Guerrero, "Secondary control strategies for frequency restoration in islanded microgrids with consideration of communication delays," *IEEE Trans. Smart Grid*, vol. 7, no. 3, pp. 1430–1441, May 2016.

[4] D. E. Olivares *et al.*, "Trends in microgrid control," *IEEE Trans. Smart Grid*, vol. 5, no. 4, pp. 1905–1919, Jul. 2014.

[5] L. Degroote, B. Renders, B. Meersman, and L. Vandevelde, "Neutral-point shifting and voltage unbalance due to single-phase dg units in low voltage distribution networks," in *Proc. IEEE Bucharest PowerTech*, Jun. 2009, pp. 1–8.

[6] R. Zhang, V. H. Prasad, D. Boroyevich, and F. C. Lee, "Three-dimensional space vector modulation for four-leg voltage-source converters," *IEEE Trans. Power Electron.*, vol. 17, no. 3, pp. 314–326, May 2002.

[7] R. Cardenas, E. Espina, J. Clare, and P. Wheeler, "Self-tuning resonant control of a seven-leg back-to-back converter for interfacing variable-speed generators to four-wire loads," *IEEE Trans. Ind. Electron.*, vol. 62, no. 7, pp. 4618–4629, Jul. 2015.

[8] X. Zhou, F. Tang, P. C. Loh, X. Jin, and W. Cao, "Four-leg converters with improved common current sharing and selective voltage-quality enhancement for islanded microgrids," *IEEE Trans. Power Del.*, vol. 31, no. 2, pp. 522–531, Apr. 2016.

[9] C. Burgos-Mellado *et al.*, "Experimental evaluation of a CPT-based four-leg active power compensator for distributed generation," *IEEE J. Emerg. Sel. Topics Power Electron.*, vol. 5, no. 2, pp. 747–759, Jun. 2017.

[10] C. Burgos-Mellado, R. Cardenas-Dobson, D. Saez, A. Costabeber, and M. Sumner, "A control algorithm based on the conservative power theory for cooperative sharing of imbalances in 4-wire systems," *IEEE Trans. Power Electron.*, vol. 34, no. 6, pp. 5325–5339, Jun. 2019.

[11] M. Savaghebi, A. Jalilian, J. C. Vasquez, and J. M. Guerrero, "Autonomous voltage unbalance compensation in an islanded droop-controlled microgrid," *IEEE Trans. Ind. Electron.*, vol. 60, no. 4, pp. 1390–1402, Apr. 2013.

[12] S. D. Swain, P. K. Ray, and K. B. Mohanty, "Improvement of power quality using a robust hybrid series active power filter," *IEEE Trans. Power Electron.*, vol. 32, no. 5, pp. 3490–3498, May 2017.

[13] F. Najafi, M. Hamzeh, and M. Fripp, "Unbalanced current sharing control in islanded low voltage microgrids," *Energies*, vol. 11, no. 10, 2018, Art. no. 2776. [Online]. Available: http://www.mdpi.com/1996-1073/11/10/2776

[14] A. Mortezaei, M. G. Simoes, M. Savaghebi, J. M. Guerrero, and A. Al-Durra, "Cooperative control of multi-master-slave islanded microgrid with power quality enhancement based on conservative power theory," *IEEE Trans. Smart Grid*, vol. 9, no. 4, pp. 2964–2975, Jul. 2018.

[15] M. Savaghebi, A. Jalilian, J. C. Vasquez, and J. M. Guerrero, "Secondary control for voltage quality enhancement in microgrids," *IEEE Trans. Smart Grid*, vol. 3, no. 4, pp. 1893–1902, Dec. 2012.

[16] L. Meng, F. Tang, M. Savaghebi, J. C. Vasquez, and J. M. Guerrero, "Tertiary control of voltage unbalance compensation for optimal power quality in islanded microgrids," *IEEE Trans. Energy Convers.*, vol. 29, no. 4, pp. 802–815, Dec. 2014.

[17] Q. Liu, Y. Tao, X. Liu, Y. Deng, and X. He, "Voltage unbalance and harmonics compensation for islanded microgrid inverters," *IET Power Electron.*, vol. 7, no. 5, pp. 1055–1063, May 2014.

[18] P. Cheng, C. Chen, T. Lee, and S. Kuo, "A cooperative imbalance compensation method for distributed-generation interface converters," *IEEE Trans. Ind. Appl.*, vol. 45, no. 2, pp. 805–815, Mar. 2009.

[19] G. Azevedo, P. Rodriguez, J. Rocabert, M. Cavalcanti, and F. Neves, "Voltage quality improvement of microgrids under islanding mode," in *Proc. IEEE Energy Convers. Congr. Expo.*, Sep. 2010, pp. 3169–3173.

[20] J. M. Guerrero, J. C. Vasquez, J. Matas, L. G. de Vicuna, and M. Castilla, "Hierarchical control of droop-controlled ac and dc microgrids—A general approach toward standardization," *IEEE Trans. Ind. Electron.*, vol. 58, no. 1, pp. 158–172, Jan. 2011.

[21] R. Pena, R. Cardenas, J. Proboste, J. Clare, and G. Asher, "Wind-diesel generation using doubly fed induction machines," *IEEE Trans. Energy Convers.*, vol. 23, no. 1, pp. 202–214, Mar. 2008.

[22] F. Tang, X. Zhou, L. Meng, J. M. Guerrero, and J. C. Vasquez, "Secondary voltage unbalance compensation for three-phase four-wire islanded microgrids," in *Proc. IEEE 11th Int. Multi-Conf. Syst., Signals Devices*, Feb. 2014, pp. 1–5.
[23] R. Guzman, L. G. de Vicuna, J. Morales, M. Castilla, and J. Miret, "Model-based active damping control for three-phase voltage source inverters with LCL filter," *IEEE Trans. Power Electron.*, vol. 32, no. 7, pp. 5637–5650, Jul. 2017.
[24] A. Aapro, T. Messo, T. Roinila, and T. Suntio, "Effect of active damping on output impedance of three-phase grid-connected converter," *IEEE Trans. Ind. Electron.*, vol. 64, no. 9, pp. 7532–7541, Sep. 2017.
[25] C. Blanco, D. Reigosa, F. Briz, and J. M. Guerrero, "Quadrature signal generator based on all-pass filter for single-phase synchronization," in *Proc. IEEE Energy Convers. Congr. Expo.*, Sep. 2014, pp. 2655–2662.
[26] T. Thacker, R. Wang, D. Dong, R. Burgos, F. Wang, and D. Boroyevich, "Phase-locked loops using state variable feedback for single-phase converter systems," in *Proc. 24th Annu. IEEE Appl. Power Electron. Conf. Expo.*, Feb. 2009, pp. 864–870.
[27] F. Xiao, L. Dong, L. Li, and X. Liao, "A frequency-fixed SOGI-based PLL for single-phase grid-connected converters," *IEEE Trans. Power Electron.*, vol. 32, no. 3, pp. 1713–1719, Mar. 2017.
[28] R. Cardenas, R. Pena, J. Proboste, G. Asher, J. Clare, and P. Wheeler, "MRAS observers for sensorless control of doubly-fed induction generators," in *Proc. 4th IET Conf. Power Electron., Mach. Drives*, Apr. 2008, pp. 568–572.
[29] A. G. Yepes, F. D. Freijedo, O. Lopez, and J. Doval-Gandoy, "Analysis and design of resonant current controllers for voltage-source converters by means of nyquist diagrams and sensitivity function," *IEEE Trans. Ind. Electron.*, vol. 58, no. 11, pp. 5231–5250, Nov. 2011.
[30] R. Cardenas, C. Juri, R. Pena, J. Clare, and P. Wheeler, "Analysis and experimental validation of control systems for four-leg matrix converter applications," *IEEE Trans. Ind. Electron.*, vol. 59, no. 1, pp. 141–153, Jan. 2012.

Enrique Espina (S'17) was born in Santiago, Chile. He received the B.Sc. degree in electrical engineering from the University of Santiago, Santiago, Chile, in 2013, the M.Sc. degree in electrical engineering, in 2017, from the University of Chile, Santiago, Chile, where he is currently working toward the Ph.D. degree in electrical engineering.

His main research interests include the control of hybrid microgrids, renewable energies, and power electronic converters.

Roberto Cárdenas-Dobson (S'95–M'97–SM'07) was born in Punta Arenas, Chile. He received the B.S. degree from the University of Magallanes, Punta Arenas, Chile, in 1988, and the M.Sc. and Ph.D. degrees from the University of Nottingham, Nottingham, U.K., in 1992 and 1996, respectively.

From 1989 to 1991 and 1996 to 2008, he was a Lecturer with the University of Magallanes. From 1991 to 1996, he was with the Power Electronics Machines and Control Group, University of Nottingham. From 2009 to 2011, he was with the Electrical Engineering Department, University of Santiago, Santiago, Chile. He is currently a Full Professor in power electronics and drives with the Electrical Engineering Department, University of Chile, Santiago. His main interests include control of electrical machines, variable speed drives, and renewable energy systems.

Prof. Cardenas is an Associate Editor for the IEEE TRANSACTIONS ON INDUSTRIAL ELECTRONICS.

Mauricio Espinoza-B. (S'15) was born in Alajuela, Costa Rica. He received the B.Sc. and Lic. degrees in electrical engineering from the University of Costa Rica, San Pedro, Costa Rica, in 2010 and 2012, respectively, and the Ph.D. degree in electrical engineering from the University of Chile, Santiago, Chile, in 2018.

From 2010 to 2019, he was a Lecturer with the University of Costa Rica. During his career, he has worked in research projects related to modular multilevel converters, machine modeling, and control systems for power electronics.

Claudio Burgos-Mellado (S'17–M'19) was born in Cunco, Chile. He received the B.Sc. and M.Sc. degrees in electrical engineering from the University of Chile, Santiago, Chile, in 2012 and 2013, respectively, and the dual Ph.D. degree in electrical and electronic engineering from the University of Nottingham, U.K., and in electrical engineering from the University of Chile, in 2019.

His current interests include battery energy storage systems, electrical vehicle technologies, power electronics, microgrids, power quality, and power theories.

Doris Sáez (S'93–M'96–SM'05) was born in Panguipulli, Chile. She received the M.Sc. and Ph.D. degrees in electrical engineering from the Ponticia Universidad Católica de Chile, Santiago, Chile, in 1995 and 2000, respectively.

She is currently a Full Professor with the Department of Electrical Engineering, University of Chile, Santiago, Chile. Her research interests include predictive control, fuzzy control design, fuzzy identification, control of power generation plants, and control of transport systems.

Prof. Sáez is an Associate Editor for the IEEE TRANSACTIONS ON FUZZY SYSTEMS and the IEEE CONTROL SYSTEMS MAGAZINE.